Analysis of all-optical switching in bacteriorhodopsin

Sukhdev Roy*,†, C. P. Singh* and K. P. J. Reddy#

*Department of Physics and Computer Science, Dayalbagh Educational Institute (Deemed University), Agra 282 005, India
#Department of Aerospace Engineering, Indian Institute of Science, Bangalore 560 012, India

All-optical switching has been demonstrated in bacteriorhodopsin (bR) based on nonlinear, intensity-induced excited state absorption. The transmission of a cw probe laser beam at 640 nm corresponding to the peak absorption of *O*-state through a bR film, is switched by a pulsed pump laser beam at 570 nm that corresponds to the maximum initial *B*-state absorption. The switching characteristics have been analysed using the rate equation approach and the six intermediate states in the bR photocycle. The effect of various parameters such as pump pulse width and intensity, rate constants of *M* and *O* states and absorption cross-section of the *B*-state at probe wavelength on switching, have been analysed in detail. It has been shown that the probe laser beam can be completely switched off by the pump laser beam at relatively low pump powers, if the *B*-state does not absorb the probe beam.

RECENT years have witnessed tremendous research effort in designing high-speed, ultrahigh bandwidth communication systems and computers. The present challenge is therefore to have all-optical information processing. The anticipated demand for this powerful capability has given the impetus to investigate new, novel nonlinear materials to enable 'light to control light'. All-optical switching is thus of primary importance for all-optical communication and computing[1].

Current interest has focused on the design of all-optical molecular devices that offer advantages of small size and weight, high intrinsic speed, extremely low propagation delay and power dissipation, and the ability to tailor properties to suit specific applications[2–5].

The photochromic retinal protein bacteriorhodopsin (bR) contained in the purple membrane fragments of *Halobacterium halobium*, has emerged as an excellent material for bio-molecular photonic applications due to its unique advantages[5–9]. It exhibits high quantum efficiency of converting light into a state change, large absorption cross-section and nonlinearities, robustness to degeneration by environmental perturbations, high stability towards photo-degradation and temperature, response in the visible spectrum, low production cost, environment-friendliness, capability to form thin films in polymers and gels, and flexibility to tune its kinetic and spectral properties by genetic engineering techniques, for device applications[5–15].

By absorbing green–yellow light, the wild-type bR molecule undergoes several structural transformations in a complex photocycle that generates a number of intermediate states[5–16]. The main photocycle of bR is as shown in Figure 1. After excitation with green–yellow light at 570 nm, the molecules in the initial *B*-state get transformed into *J*-state within about 0.5 ps. The species in the *J*-state thermally transforms in 3 ps into the intermediate *K*-state, which in turn transforms in about 2 μs into the *L*-state. From the *L*-state, bR thermally relaxes to the M^{I}-state within 8 μs and undergoes irreversible transition to the M^{II}-state. The molecules then relax through the *N* and *O* intermediates to the initial *B*-state within about 10 ms. An important feature of all the intermediate states is their ability to be photo-chemically switched back to the initial *B*-state by shining light at a wavelength that corresponds to the absorption peak of the intermediate in question. The wavelength in nm of the absorption peak of each species is shown as a subscript in Figure 1.

Various applications have been proposed based on its proton transport, photoelectric and photochromic properties such as targeted drug delivery to bio-catalytic reactors, fuel cells, nano-machines, desalination of sea water, conversion of sunlight to electricity, ultrafast light detection, chemo- and bio-sensing, artificial retinas, photon counters, photo-voltaic converters, pattern recognition systems, information recording, associative and 3D memories, holography, second harmonic generation, saturable absorption, wave mixing, phase conjugation, nonlinear optical filtering, transient gratings, interferometric systems, optical bistability, mode locking, optical limiting, spatial light modulation, optical image processing, neural networks, incoherent to coherent conversion,

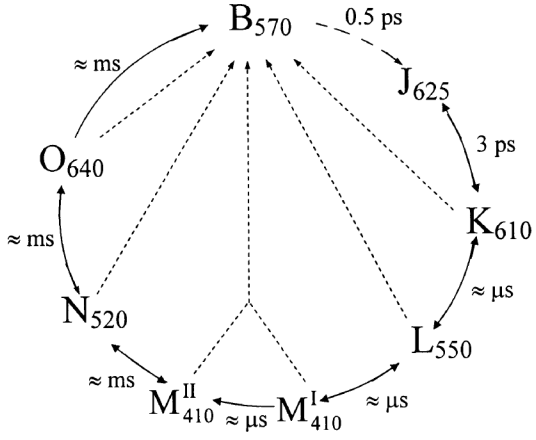

Figure 1. Schematic of the photochemical cycle of bR molecule. Subscripts indicate absorption peaks in nm. Solid and dashed arrows represent thermal and photo-induced transitions respectively.

†For correspondence. (e-mail: sukhdevr@hotmail.com)

optical displays, optical computing, logic gates and beam deflection[5–16].

In this communication, we demonstrate all-optical switching in bR molecules based on nonlinear, intensity-induced excited-state absorption of a cw probe laser beam at 640 nm by a pulsed pump laser beam at 570 nm[17–21]. The switching characteristics have been analysed using the rate equation approach and the six intermediate states in the bR photocycle. The effect of the variation of pump pulse width, pump intensity, rate constants of M and O intermediate states and absorption cross-section of the B-state at 640 nm on the switching characteristics have been analysed to achieve large percentage modulation and low power operation.

The photochemical cycle of bR molecules, can be represented by the simple rate-equation approach in terms of the population densities in the various intermediate states. The J-state has been neglected in this simplified model, since it has an extremely short lifetime of 3 ps compared to the other states. To simplify the analysis, forward transitions between different intermediate states and a single M-state have been considered, as both M^{I} and M^{II} states are spectroscopically identical[5–16].

We consider bR molecules exposed to a light beam of intensity I'_{m}, which modulates the population densities of different states through the excitation and de-excitation processes, and can be described by the rate equations in the following form,

$$\frac{\mathrm{d}N}{\mathrm{d}t} = \hat{O}N, \tag{1}$$

where $\hat{O}$ operator is defined in terms of the photo-induced and thermal transitions of different states as,

$$\hat{O} = \begin{pmatrix} -I_{\mathrm{m}}\sigma_{\mathrm{B}}\psi_{\mathrm{BK}} & I_{\mathrm{m}}\sigma_{\mathrm{K}}\psi_{\mathrm{KB}} & I_{\mathrm{m}}\sigma_{\mathrm{L}} \\ I_{\mathrm{m}}\sigma_{\mathrm{B}}\psi_{\mathrm{BK}} & -(k_{\mathrm{K}} + I_{\mathrm{m}}\sigma_{\mathrm{K}}\psi_{\mathrm{KB}}) & 0 \\ 0 & k_{\mathrm{K}} & -(k_{\mathrm{L}} + I_{\mathrm{m}}\sigma_{\mathrm{L}}) \\ 0 & 0 & k_{\mathrm{L}} \\ 0 & 0 & 0 \\ 0 & 0 & 0 \end{pmatrix}$$

$$\begin{pmatrix} I_{\mathrm{m}}\sigma_{\mathrm{M}} & I_{\mathrm{m}}\sigma_{\mathrm{N}} & k_{\mathrm{O}} + I_{\mathrm{m}}\sigma_{\mathrm{O}} \\ 0 & 0 & 0 \\ 0 & 0 & 0 \\ -(k_{\mathrm{M}} + I_{\mathrm{m}}\sigma_{\mathrm{M}}) & 0 & 0 \\ k_{\mathrm{M}} & -(k_{\mathrm{N}} + I_{\mathrm{m}}\sigma_{\mathrm{N}}) & 0 \\ 0 & k_{\mathrm{N}} & -(k_{\mathrm{O}} + I_{\mathrm{m}}\sigma_{\mathrm{O}}) \end{pmatrix}, \tag{2}$$

and the transpose of the population vector **N** is given by

$$\tilde{N} = (N_{\mathrm{B}}, N_{\mathrm{K}}, N_{\mathrm{L}}, N_{\mathrm{M}}, N_{\mathrm{N}}, N_{\mathrm{O}}), \tag{3}$$

where I_{m} is the photon density flux of the modulation laser beam, i.e. ratio of the intensity I'_{m} to the photon energy $h\nu$, σ and k are the absorption cross-sections and rate constants respectively, of different states denoted by the respective subscripts and $\psi_{\mathrm{BK}} = \psi_{\mathrm{KB}} = 0.64$ are the quantum efficiencies for the transitions $B \rightarrow K$ and $K \rightarrow B$, respectively. The typical values of the constants and absorption cross-sections for various levels at different wavelengths are given in Table 1 (refs 5, 6, 9–14).

We consider a pulsed pump laser beam at 570 nm and a weak cw probe laser beam at 640 nm, corresponding to the peak absorption of the initial B and the intermediate O-state respectively. The transmitted intensity of the probe beam which is initially high (switch-on state) due to lower linear absorption is switched low (switch-off state) when a pulsed laser beam pumps the sample, enhancing the population of the O-state. The propagation of the probe beam through the bR medium is governed by,

$$\frac{\mathrm{d}I_{\mathrm{p}}}{\mathrm{d}x} = -\alpha_{\mathrm{p}}(I_{\mathrm{m}})I_{\mathrm{p}}, \tag{4}$$

where α_{p} is the nonlinear intensity-dependent absorption coefficient of the probe beam written here as,

$$\alpha_{\mathrm{p}}(I_{\mathrm{m}}) = N_{\mathrm{B}}(I_{\mathrm{m}})\sigma_{\mathrm{Bp}} + N_{\mathrm{K}}(I_{\mathrm{m}})\sigma_{\mathrm{Kp}} + N_{\mathrm{O}}(I_{\mathrm{m}})\sigma_{\mathrm{Op}}, \tag{5}$$

where σ is the absorption cross-section of the state denoted by the subscript and p denotes the value at probe wavelength. The modulating pump laser pulse is given by[17,18],

$$I'_{\mathrm{m}} = I'_{\mathrm{m0}} \exp\left(-c\left(\frac{t - t_{\mathrm{m}}}{\Delta t}\right)^2\right), \tag{6}$$

where $c = 4 \ln 2$ is the pulse profile parameter and Δt is the pulse width.

The optical switching curves, namely the probe transmission intensity as a function of time have been obtained by solving rate equations for the intermediate states through computer simulations using eqs (1)–(6) with the typical values of the rate constants and absorption cross-sections given in Table 1, with film thickness of 30 μm. Figure 2 shows that the switch-on/off time and percentage modulation (i.e. variation in the normalized transmitted intensity of the probe beam ($I_{\mathrm{pout}}/I_{\mathrm{pin}}$) when it

Table 1. Typical values of rate constants and absorption cross-sections[5,6,9–14]

Rate constant	Value (s^{-1})	Absorption cross-section	Value (cm^2)	
			570 nm	640 nm
		σ_{B}	2.4×10^{-16}	0.3×10^{-16}
k_{K}	5.0×10^{5}	σ_{K}	1.8×10^{-16}	1.4×10^{-16}
k_{L}	2.0×10^{4}	σ_{L}	1.5×10^{-16}	–
k_{M}	1.0×10^{3}	σ_{M}	0.0	–
k_{N}	3.3×10^{2}	σ_{N}	1.7×10^{-16}	–
k_{O}	2.0×10^{2}	σ_{O}	1.1×10^{-16}	2.5×10^{-16}

is on and off), increase with increase in pulse width (Δt), with the modulation level saturating after a certain value. For instance, for $\Delta t = 1$ ms, the switch-off/on time is 4 ms and 25 ms respectively, with percentage modulation of 9% as shown in Figure 2. For $\Delta t = 5$ ms, the switch-off/on time is 9 ms and 30 ms respectively, with percentage modulation of 18%. This can be achieved with a 5 nW laser focused to a 5 μm^2 spot size. The symmetry of the curves expectedly increases for Δt greater than the relaxation time of the complete bR photocycle, as this conforms to the steady state case. The inset in Figure 2 shows the corresponding dynamic and steady state variations for $\Delta t = 30$ ms. The percentage modulation and the symmetry of the curves are almost identical with a delay of about 4.3 ms in the dynamic case, as this corresponds to the time taken by the molecules to populate the *O*-state[18]. Peak pumping intensity required to get the same percentage modulation increases for smaller Δt values. For Δt =10 μs and 10 ns, $I'_{m0} = 30$ W/cm^2 and 30 kW/cm^2 respectively for a percentage modulation of 17%.

The kinetic and spectral properties of bR can be altered through biotechnological procedures such as variation in the polymer environment, including pH, temperature, degree of hydration and addition of chemicals[5–14]. For instance, the protonation of Schiff base group and the configuration of the retinylidene residue affect the position of the absorption bands[6].

Figure 3 shows the variation in the normalized probe beam transmission with time, for different values of the absorption cross-section of the *B*-state at the probe wavelength (σ_{Bp}). As σ_{Bp} decreases, the percentage modulation increases drastically, as it results in decrease in absorption of probe laser beam. For $\sigma_{Bp} = 0.3 \times 10^{-16}$ cm^2, 0.1×10^{-16} cm^2 and 0, the transmittance gets modulated by 22%, 60% and 96% respectively, for peak pumping intensity $I'_{m0} = 0.4$ W/cm^2. A 50% modulation of the probe beam for $\sigma_{Bp} = 0$, requires a lower intensity $I'_{m0} = 38$ mW/cm^2. Hence, for a given Δt, increasing the pump intensity leads to an increase in the percentage modulation. The probe beam can be completely switched-off by increasing the population of the *O*-state, i.e. reducing k_O and having $\sigma_{Bp} = 0$. For $\Delta t = 5$ ms and 10 ms with $k_O = 100$ s^{-1}, 100% modulation can be achieved with $I'_{m0} = 0.9$ W/cm^2 and 0.5 W/cm^2 respectively.

The lifetime of the *M*-state ($\tau_M = k_M^{-1}$) can be prolonged by several orders of magnitude (from microseconds to minutes), in dried polymer-based films of bR that have been treated with organic amines [e.g. diaminopropane (Sigma D2360-2) or guanidine hydrochloride (Sigma G7153)][10]. The *O*-state lifetime ($\tau_O = k_O^{-1}$) can also be prolonged by inhibiting proton release via pH adjustment to 6–6.5 and adding glycerol[10].

The effect of variation in the rate constants k_M and k_O on the switching characteristics is shown in Figure 4. As k_M increases, the switching time decreases and percentage modulation increases. This happens as an increase in k_M leads to rapid increase in the population of the *O*-state, resulting in increased absorption and lower switch-on/off time. For $k_M = 200$ s^{-1}, the switch-off/on time is 18 ms and 39 ms respectively, resulting in 17% modulation, while for $k_M = 1000$ s^{-1}, the switch-off/on time is 18 ms and 36 ms, resulting in 20% modulation of the probe beam. On the other hand, as k_O increases, both the switching time and percentage modulation decrease, as shown in Figure 4 with dashed lines. Increase in k_O results in a faster decay from the *O* to the initial *B*-state, thereby reducing the *O*-state population and hence lowering the absorption of the probe beam. For $k_O = 400$ s^{-1}, the switch-off and switch-on time are 17 ms and 25 ms respectively, resulting in 16% modulation, while for $k_O = 100$ s^{-1}, the switch-off/on time is 19 ms and 64 ms respectively, with 22% modulation of the probe laser

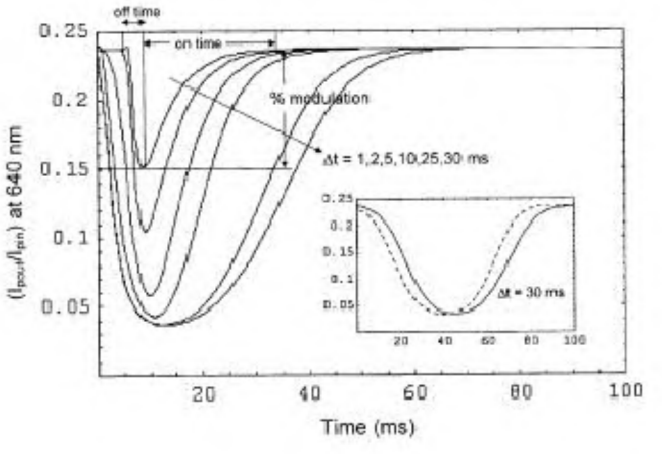

Figure 2. Variation of normalized transmitted intensity of the probe beam (I_{pout}/I_{pin}) at 640 nm with time, for different pump pulse width (Δt) values for $I'_{m0} = 100$ mW/cm^2, $\sigma_{Bp} = 0.3 \times 10^{-16}$ cm^2, $t_m = 6$ ms and $k_M = 1.0 \times 10^3$ s^{-1}. (Inset) Corresponding variation for steady state (dashed line) and dynamic (solid line) case for $\Delta t = 30$ ms and $t_m = 40$ ms.

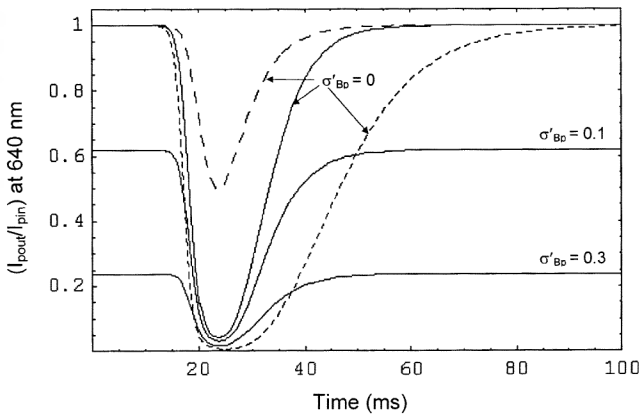

Figure 3. Variation of normalized transmitted intensity of the probe beam (I_{pout}/I_{pin}) at 640 nm with time, with $\Delta t = 5$ ms, $t_m = 20$ ms and $k_M = 1.0 \times 10^3$ s^{-1}. ——— $k_O = 200$ s^{-1}, $I'_{m0} = 0.4$ W/cm^2 and $\sigma_{Bp} = \sigma'_{Bp} \times 10^{-16}$ cm^2; – – – – $\sigma_{Bp} = 0$, $k_O = 200$ s^{-1}, $I'_{m0} = 38$ mW/cm^2; - - - - $\sigma_{Bp} = 0$, $k_O = 100$ s^{-1}, $I'_{m0} = 0.9$ W/cm^2.

beam. The curves become more symmetric with increase in k_M and k_O values, as relaxation time of bR photocycle becomes smaller than the pulse width.

The proposed configuration corresponds to an inverter (NOT) logic gate, since the probe beam intensity as the output is high when the input pump intensity is low, and the output is low when the input is high, as shown in Figure 5 (refs 17–21). The normalized transmitted intensity of the probe laser beam would be minimum at maximum absorption, i.e. when the population of the *O*-state is maximum leading to the switch-off state. As is evident from Figure 5, there is a time delay of about 4.3 ms between the pump laser profile and the transmitted probe laser profile that corresponds to the time taken by the molecules in the photocycle to go from the initial *B*-state to populate the *O*-state[18]. This basic switching characteristic and configuration can be used to design all-optical universal NOR and NAND logic gates with multiple pump pulses, which would be reported elsewhere.

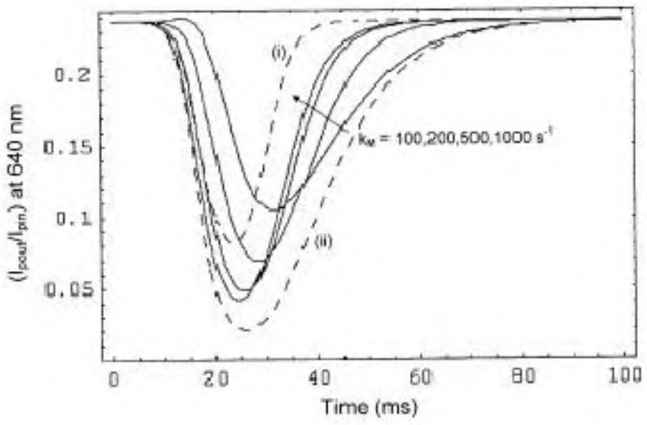

Figure 4. Variation on normalized transmitted intensity of the probe beam (I_{pout}/I_{pin}) at 640 nm with time, for Δt = 10 ms, I'_{m0} = 100 mW/cm^2, t_m = 20 ms and $\sigma_{Bp} = 0.3 \times 10^{-16}$ cm^2. ——— k_O = 200 s^{-1}; (i) – – – – k_m = 1000 s^{-1} and k_O = 400 s^{-1}; (ii) – – – – k_m = 1000 s^{-1} and k_O = 100 s^{-1}.

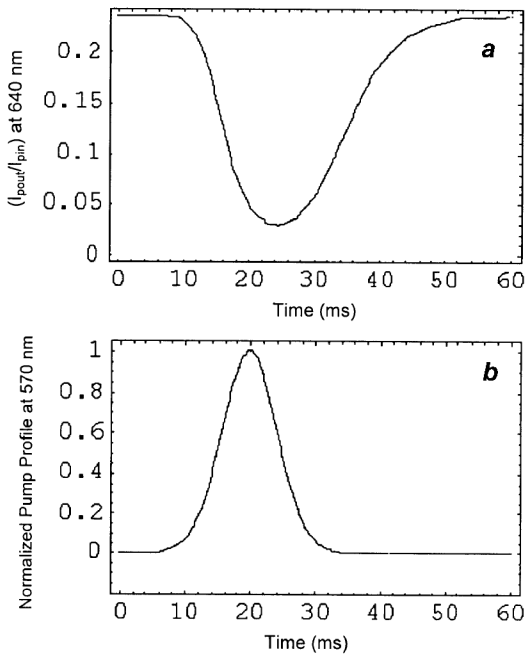

Figure 5. All-optical inverter (NOT) logic gate. ***a***, Variation of normalized transmitted intensity of the probe beam (I_{pout}/I_{pin}) at 640 nm with time; and ***b***, Normalized input pump pulse profile.

Complete switching at low powers and low switching time can be achieved if the probe beam is not absorbed by the initial *B*-state (σ_{Bp} = 0), and if k_M is large and k_O is small. The modulation level can also be controlled by adjusting the pump intensity. Since the properties of the bR molecule such as the relaxation rates, absorption cross-sections and spectra of the intermediate states can be modified by chemical or genetic engineering techniques, the switching characteristics of bR can be tailored for desired applications[4–14]. Since bR can also be processed as a film or in a crystalline form for 2D/3D applications, bR-based all-optical switches would be potentially useful in optical signal processing in optical networks. They can provide an alternative to the widely required thermo-optic, MEMS and liquid-crystal switches that operate in the ms range. As large, high-density arrays of these switches can also be fabricated, that can operate at very low switching energies with high thermal stability, they would also be useful in parallel optical computing.

We have shown an absorptive all-optical switching of a cw probe laser beam by a pulsed laser beam in bR. The switching characteristics are sensitive to variation in pump pulse width and intensity, absorption cross-section of the *B*-state at probe wavelength and rate constants of the *M* and *O*-states of the bR photocycle. The proposed all-optical switch would be useful due to advantages of small size, simple digital operation, 100% modulation at low powers, small linear absorption coefficient, mirrorless structure, and flexibility in its design.

1. Bishop, D. J., Giles, C. R. and Das, S. R., *Sci. Am.*, 2001, **284**, 88–94.
2. Raymo, F. M., *Adv. Mater.*, 2002, **14**, 401–414.
3. Roy, S., Singh C. P. and Reddy, K. P. J., *Appl. Phys. Lett.*, 2000, **77**, 2656–2658.
4. Bachtold, A., Hadley, P., Nakanishi, T. and Dekker, C., *Science*, 2001, **294**, 1317–1320.
5. Stuart, J. A., Mercy, D. L., Wise K. J. and Birge, R. R., *Synth. Met.*, 2002, **127**, 3–15.
6. Hampp, N., *Chem. Rev.*, 2000, **100**, 1755–1776.
7. Oesterhelt, D., Bräuchle, C. and Hampp, N., *Q. Rev. Biophys.*, 1991, **24**, 425–478.
8. Lanyi, J. K. and Pohorille, A., *Trends Biotechnol.*, 2001, **19**, 140–144.
9. Roy, S., Singh C. P. and Reddy, K. P. J., *J. Appl. Phys.*, 2001, **90**, 3679–3688.
10. Birge, R. R. *et al.*, *J. Phys. Chem. B*, 1999, **103**, 10746–10766.
11. Kumar, G. R., Wategaonkar, S. J. and Roy, M., *Opt. Commun.*, 1993, **98**, 127–131.
12. Reddy, K. P. J., *Appl. Phys. Lett.*, 1994, **64**, 2776–2778.
13. Reddy, K. P. J., *J. Appl. Phys.*, 1995, **77**, 6108–6113.

14. Roy, S. and Reddy, K. P. J., *Curr. Sci.*, 2000, **78**, 184–188.
15. Araujo de, R. E., Borissevitch, G. and Gomes, A. S. L., *Electron. Lett.*, 2000, **36**, 71–73.
16. Kobayashi, T., Saito, T. and Ohtani, H., *Nature*, 2001, **414**, 531–534.
17. Li, C., Zhang, L., Wang, R., Song Y. and Wang, Y., *J. Opt. Soc. Am. B*, 1993, **11**, 1356–1360.
18. Li, C., Zhang, L., Yang, M., Wang, H. and Wang, Y., *Phys. Rev. A*, 1994, **49**, 1149–1157.
19. Xu, H. *et al.*, *Mater. Res. Bull.*, 1996, **31**, 351–354.
20. Henari, F. Z., Cazzini, K. H., Weldon D. L. and Blau, W. J., *Appl. Phys. Lett.*, 1996, **68**, 619–621.
21. Henari, F. Z., *J. Opt. A; Pure Appl. Opt.*, 2001, **3**, 188–190.

ACKNOWLEDGEMENTS. This work was partially supported by the AICTE Career Award for Young Teachers, 2001 and the Department of Science and Technology, Government of India grant awarded to S.R.

Received 3 April 2002; revised accepted 1 August 2002

Nucleophile-induced dissolution of gold and silver in micelle

Tarasankar Pal
Department of Chemistry, Indian Institute of Technology, Kharagpur 721 302, India

At a given experimental condition the reduction potential (M^{n+}/M_{bulk}) of metals decreases progressively from bulk metal (number of atoms = ∞) to the metal cluster (number of atoms are a few only), and eventually attains a minimum value in the M^{n+}/M_{atom} (number of atoms = 1) case. The reduction potential of a metal is further lowered in the presence of a nucleophile. Exploiting this idea it has become possible to dissolve coinage metal particles, even gold, in micellar medium without the need of any mineral acid.

OF the three coinage metals, gold is the most stable (corrosion resistant) and copper is most vulnerable to oxidation under ambient condition. In this regard, silver occupies an intermediate position. None of these metals dissolves in water as such.

The dissolution, i.e. oxidation of noble metal (nobility due to high positive reduction potential value)[1] in the absence of any acid can be understood through the disappearance of a micro-stirrer in micellar solution.

When there is a report that gold and silver both dissolve in aqueous medium, some people may rub their eyes in disbelief. Similarly, a few chemists will not be less surprised if told that the oxidation of metal proceeds in the presence of $NaBH_4$ solution. The dissolution can be demonstrated by means of a simple experiment. Under laboratory conditions, a thin silver wire (~ 0.2 cm dia; 6 cm length), if used as a micro-stirrer gets dissolved during the course of stirring an aqueous solution (50 ml) containing excess $NaBH_4$ (0.5 g). After a few minutes of stirring, the silver wire loses its weight and ultimately dissolves in water due to the oxidation of silver, leaving Ag^+ species in the aqueous phase[2,3]. For a better visualization, common surfactants like CTAB (cetyltrimethylammonium bromide) or SDS (sodium dodecyl sulphate) or TX-100 (poly(oxyethylene)*iso*-octylphenyl ether) in the concentration range ~ 10^{-2} mol dm^{-3} have been observed to be helpful. Sonication in lieu of stirring promotes faster dissolution.

Silver dissolves in an aqueous medium containing $NaBH_4$ under ambient conditions. So it is possible! It is very much like the well-known dissolution process of silver that is carried out during the extraction of silver using cyanide/air interface. Cyanide acts as a complexing agent as well as a nucleophile.

After the dissolution of silver wire in $NaBH_4$, the colourless solution would turn yellow (absorption maximum, λ_{max} ~ 400 nm) due to the reduction of the dissolved silver ion of the micro-stirrer by excess $NaBH_4$ already present in the solution. The yellow colour is due to the micelle-stabilized silver hydrosol in the nano domain. These silver metal nano particles again could be dissolved by shaking the solution under laboratory conditions, with a little amount of $NaBH_4$ in solution[2]. The cycle of appearance/disappearance of the yellow-coloured metal sol in aqueous phase would continue as long as $NaBH_4$ remains in the solution. This is an interesting and simple example of a reversible reaction. To make the experiment cost-effective, dilute $AgNO_3$ solution (~ 10^{-3} mol dm^{-3}) in micelle and $NaBH_4$ could also be used to demonstrate the reversible reaction[2].

Similarly a micro-stirrer of gold can be dissolved in aqueous solution in the presence of a surfactant and I_2/SCN^- or I_2/I^- system without the need of aqua regia. However, oscillation will not be observed as in the case of silver[3].

The bulk property of any metal changes drastically while the particles go to the so-called neglected dimension, i.e. nano domain of the metal[4]. At a given experimental condition, the reduction potentials (M^{n+}/M_{bulk}) decrease progressively as we move from bulk metal (number of atoms = ∞) to the metal cluster (number of atoms are a few only) and eventually attain a minimum value in the M^{n+}/M_{atom} (number of atoms = 1) case[5]. Moreover, upon adsorption of a nucleophile a metal surface may further lower its reduction potential value (causing a change in Fermi potential) because of the enhancement of the electron density by the nucleophile (here it is $NaBH_4$, SCN^- and I^-) onto the metal surface[6]. Shift of Fermi level (FL) has been schematically presented in Figure 1. It has been shown that the gap

For correspondence. (e-mail: tpal@chem.iitkgp.ernet.in)